Inhibition of Sphingosine 1-Phosphate Lyase for the Treatment of Rheumatoid Arthritis: Discovery of (*E*)-1-(4-((1*R*,2*S*,3*R*)-1,2,3,4-Tetrahydroxybutyl)-1*H*-imidazol-2-yl)ethanone Oxime (LX2931) and (1*R*,2*S*,3*R*)-1-(2-(Isoxazol-3-yl)-1*H*-imidazol-4-yl)butane-1,2,3,4-tetraol (LX2932)

Jeffrey T. Bagdanoff,[†] Michael S. Donoviel,[‡] Amr Nouraldeen,[‡] Marianne Carlsen,[†] Theodore C. Jessop,[†] James Tarver,[†] Saadat Aleem,[†] Li Dong,[†] Haiming Zhang,[†] Lakmal Boteju,[†] Jill Hazelwood,[‡] Jack Yan,[†] Mark Bednarz,[†] Suman Layek,[†] Iris B. Owusu,[‡] Suma Gopinathan,[‡] Liam Moran,[‡] Zhong Lai,[†] Jeff Kramer,[‡] S. David Kimball,[†] Padmaja Yalamanchili,[†] William E. Heydorn,[†] Kenny S. Frazier,[‡] Barbara Brooks,[‡] Philip Brown,[‡] Alan Wilson,[‡] William K. Sonnenburg,[‡] Alan Main,[†] Kenneth G. Carson,[†] Tamas Oravecz,[‡] and David J. Augeri*,[†]

[†]*Lexicon Pharmaceuticals, Inc., 350 Carter Road, Princeton, New Jersey 08540, United States, and* [‡]*Lexicon Pharmaceuticals, Inc., 8800 Technology Forest Place, The Woodlands, Texas 77381, United States*

Sphingosine 1-phosphate lyase (S1PL) has been characterized as a novel target for the treatment of autoimmune disorders using genetic and pharmacological methods. Medicinal chemistry efforts targeting S1PL by direct in vivo evaluation of synthetic analogues of 2-acetyl-4(5)-(1(*R*),2(*S*),3(*R*),4-tetrahydroxybutyl)-imidazole (THI, **1**) led to the discovery of **2** (LX2931) and **4** (LX2932). The immunological phenotypes observed in S1PL deficient mice were recapitulated by oral administration of **2** or **4**. Oral dosing of **2** or **4** yielded a dose-dependent decrease in circulating lymphocyte numbers in multiple species and showed a therapeutic effect in rodent models of rheumatoid arthritis (RA). Phase I clinical trials indicated that **2**, the first clinically studied inhibitor of S1PL, produced a dose-dependent and reversible reduction of circulating lymphocytes and was well tolerated at dose levels of up to 180 mg daily. Phase II evaluation of **2** in patients with active rheumatoid arthritis is currently underway.

Introduction

Research dedicated to the study of sphingosine signaling pathways identified sphingosine 1-phosphate lyase (S1PL[a]) as an important enzyme involved in the regulation of the immune system.[1] Human S1PL is an intracellular protein composed of 568 amino acids and bears 91% similarity to its mouse homologue. The N-terminus is anchored in the membrane-rich endoplasmic reticulum (ER). The C-terminus contains the catalytic site that extends into the cytosol and performs an irreversible retro-aldol degradation of sphingosine 1-phosphate (S1P), a key signaling lipid present in all mammalian cells. S1P can serve both as an extracellular signal and as a secondary messenger in biochemical pathways that regulate cell differentiation and apoptosis as well as the vascular and immune systems.[2] S1P is an extracellular ligand for a family of five G-protein-coupled receptors (GPCR) termed S1P1−S1P5, which are expressed in many tissues.[3] To date, the majority of the research aimed at pharmacological intervention of the S1P signaling pathway has focused on synthetic agonists of S1P receptors (S1PR), in particular S1P1, which regulates numerous aspects of immune function including T- and B-cell trafficking.[2,3] This approach serves to mimic the endogenous effects of S1P and was led by the discovery of Fingolimod (FTY720),[4] recently approved for the treatment of multiple sclerosis by the FDA.

A functional consequence of S1P or Fingolimod binding to and activation of S1P1 is receptor internalization and intracellular degradation.[5] This so-called functional antagonism of S1P1 eventually leads to inhibition of lymphocyte egress from secondary immune tissues, resulting in peripheral lymphopenia and immunosuppression. Inhibition of S1PL increases tissue S1P content that leads to similar immunomodulatory effects.[1c,6] The mechanism likely involves the action of both intracellular and extracellular S1P and may not be limited to functional antagonism of S1PR or inhibition of lymphocyte recirculation. A somewhat surprising result of the analysis of mice and rats expressing reduced levels of S1PL activity was that significant increases in tissue S1P concentrations were observed predominantly in lymphoid tissues and that mice expressing less than 10% wild type S1PL exhibited lymphopenia without other overt physiological effects.[1a] The relative tissue specificity of S1PL inhibition suggested that targeting this enzyme may provide an attractive alternative approach to modulation of S1P receptors by synthetic ligands that presumably achieve systemic circulation and wide tissue distribution following administration.

S1PL-deficient mice showed resistance to various inflammatory and autoimmune challenges, indicating that pharmacological inhibition of S1PL represents a novel therapeutic strategy for the treatment of autoimmune disorders.[1a,7] We recently reported a series of small molecules that, when administered

---

*To whom correspondence should be addressed. Phone: (609) 466-5526. Fax: (609) 466-6079. E-mail: daugeri@lexpharma.com.

[a]Abbreviations: S1P, sphingosine 1-phosphate; S1PL, sphingosine 1-phosphate lyase; KO, knockout; S1P1, sphingosine 1-phosphate receptor 1; S1PR, sphingosine 1-phosphate receptor; GPCR, G-protein-coupled receptor; CBC, complete blood count; SAR, structure−activity relationship; ADME, absorption, distribution, metabolism, excretion; CIA, collagen induced arthritis; RA, rheumatoid arthritis; ER, endoplasmic reticulum; NK cells, natural killer cells; ECG, electrocardiogram; AUC, area under curve; PK-PD, pharmacokinetic-pharmacodynamic.

Scheme 1[a]
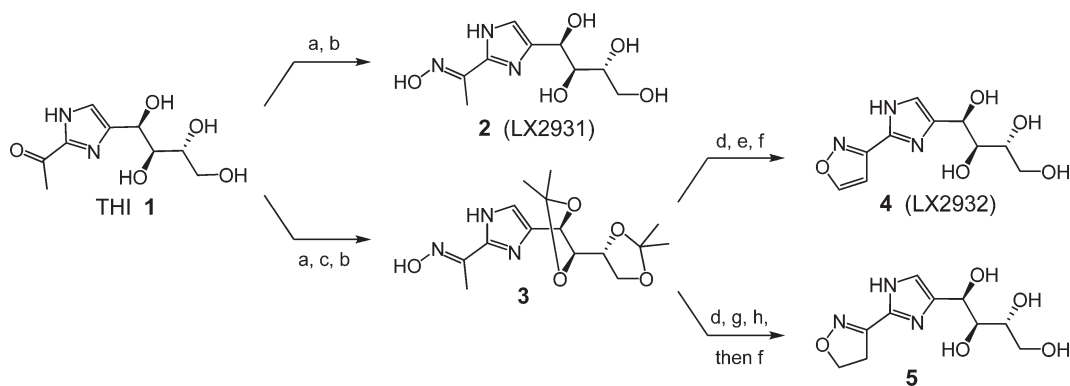
[a] Conditions: (a) 1.0 equiv HCl, Ph₃CONH₂, dioxane:water (2:1); (b) 2.0 M HCl in dioxane; (c) 2,2-dimethoxypropane, DCM, *p*-TsOH·H₂O; (d) *n*-BuLi, −78 °C, THF, then DMF; (e) (CF₃CO)₂O, TEA, DCM; (f) dioxane:1 N aq HCl (1:1), 50 °C; (g) NaBH₄, MeOH, 0 °C; (h) Ph₃P, I₂, TEA, THF.

Scheme 2[a]
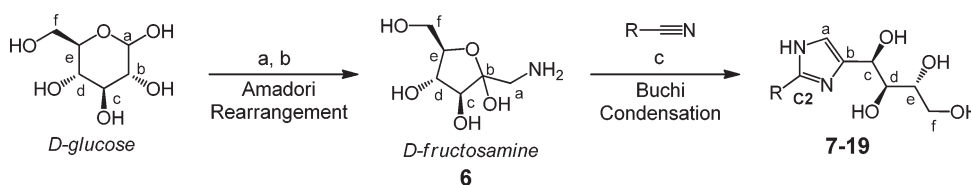
[a] Conditions: (a) Bn₂NH, EtOH, HOAc, 80 °C; (b) H₂, Pd−C, EtOH, HOAc; (c) *R*-nitrile, MeONa, MeOH, then HOAc.

orally to mice, recapitulated the immune phenotype of S1PL deficiency.[8] Herein, we describe the research effort that led to the identification of compounds **2** and **4**. Compound **2** is the first clinically studied inhibitor of S1PL for the treatment of rheumatoid arthritis.

Chemistry

As shown in Scheme 1, a number of investigational analogues were generated from 2-acetyl-4(5)-(1(*R*),2(*S*),3(*R*),4-tetrahydroxybutyl)-imidazole (THI, **1**). Condensation of **1** with *O*-trityl hydroxylamine followed by removal of the trityl protecting group afforded **2** exclusively as the configurationally pure *E*-oxime. Ketalization of the tetraol side chain prior to selective deprotection of the trityl group under anhydrous acidic conditions provided bis-ketal **3**. Subsequent deprotonation of oxime **3** and alkylation of the aza-enolate with *N,N*-dimethylformamide provided isoxazole **4** after aromatization and deprotection of the tetraol side chain. Alternatively, reduction of the intermediate *N,N*-dimethylformamide addition product followed by cyclization furnished dihydroisoxazole **5** after deprotection of the tetraol side chain.

A method for rapidly generating variously substituted C2-heterocycles was adapted from the Amadori rearrangement[9] and Buchi cyclization[10] methods (Scheme 2). In the Amadori rearrangement, reaction of D-glucose with dibenzylamine under mildly acidic conditions provided, after hydrogenolysis of the benzyl groups, D-fructosamine acetate **6**. Subsequent Buchi condensation of the aza-sugar with imidates generated from nitriles and sodium methoxide provided heterobicyclic tetraols **7−19**. We have previously reported synthetic methods for altering the side chain and substituting the core heterocycle present in this chemotype represented by **1**.[8] In that disclosure, it was determined that good chemical yields in the Buchi cyclization were obtained only when fructosamine·HOAc, the aza-sugar derived from naturally occurring D-glucose, was utilized. While this phenomenon has not been extensively

investigated, synthetic studies in our own laboratories involving deuterated solvents have elucidated certain mechanistic nuances of the venerable Buchi cyclization.[11]

Results and Discussion

During the course of synthetic investigations with **1**, we noticed the formation of aldol side products that result from enolization of the ketone, even under mildly acidic conditions (Scheme 3). Upon concentration of various HPLC purified ketone containing analogues from a mixture of acetonitrile and water buffered with ammonium acetate, the aldol adduct **20** was routinely detected by LCMS and NMR in variable but significant quantities. By contrast, oxime **2** was found to be more stable under conditions that proved problematic for the ketone present in **1**. The relative reactivity of the ketone of **1** versus **2** is illustrated by Scheme 3. Treatment of **1** with dilute DCl in excess D₂O provides deuterated intermediate *d₈*-**1** due to facile enolization of the ketone. However, after trapping the reactive ketone as oxime *d₃*-**2**, no enolization was observed under protic aqueous conditions. No loss of deuterium content, dimerization, erosion of oxime geometry, or other decomposition was observed upon standing in 1.0 M aqueous HCl at 40 °C for up to two weeks. In contrast to ketone **1**, compound **2** displayed enhanced solubility properties as the free base and showed extended solubility as the HCl salt; the HCl salt was readily formulated in neutral water.

We have previously determined that peak lymphopenia occurred between 12 and 24 h following oral administration of **1** to mice.[8] Accordingly, 18 h after oral administration of a 30 mg/kg dose of **2**, the resulting lymphocyte reduction in peripheral blood was measured by complete blood cell count (CBC) analysis. As shown in Table 1, regiochemically pure *E*-oxime **2** lowered peripheral lymphocyte counts by 60% as compared to vehicle control. To further clarify the effect of the structural transformation on in vivo activity, the pharmacokinetic profile was obtained from a separate PK study.

Scheme 3[a]
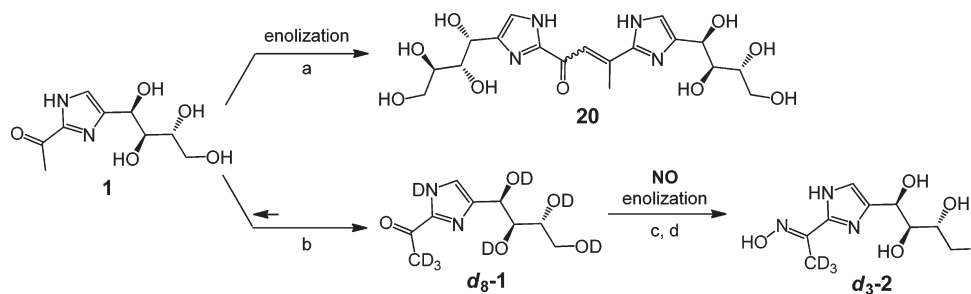
[a] Conditions: (a) NH₄OAc, MeCN, water; (b) 1.0 M DCl in D₂O; (c) Ph₃CONH₂, 1.0 M DCl in D₂O, dioxane; (d) 4.0 M HCl in dioxane, water.

Table 1. SAR of C-2 Substituted Imidazoles Containing sp^2-Hybridized Heteroatoms

1 — -25 %[a], 15.0 μM·h[b]	**8** — -4 %, 5.3 μM·h	**12** — -2 %, 10.3 μM·h	**16** — -10 %, 5.9 μM·h
2 — -60 %, 8.8 μM·h	**9** — -39 %, 12.5 μM·h	**13** — +2 %, 7.8 μM·h	**17** — -6 %, 11.7 μM·h
4 — -70 %, 21.0 μM·h	**10** — -19 %, 9.6 μM·h	**14** — -26 %, 9.1 μM·h	**18** — -27 %, 8.2 μM·h
5 — -12 %, 8.3 μM·h	**11** — -30 %, 12.8 μM·h	**15** — -7 %, 6.1 μM·h	**19** — -55 %, 26.9 μM·h

[a] Reported as % change in circulating lymphocyte numbers relative to vehicle control 18 h after oral delivery of 30 mg/kg dose of HCl salt to mice ($n = 5$). [b] $AUC_{t_0 \rightarrow \text{infinity}}$ following 10 mg/kg oral dose to mice ($n = 4$). For AUC data for **2** and **4**, see Table 2 for complete data (including SD) from multiple experiments.

Table 2. Pharmacokinetic Parameters of **2** and **4** in Mice[a]

compd	$T_{1/2}$[b]	C_{max}[c]	T_{max}[d]	Vss[e]	Cl[f]	AUC[g]	%F[h]
2	1.6 ± 0.3	3.6 ± 1.2	0.45 ± 0.1	0.9 ± 0.4	7.6 ± 1.1	8.8 ± 1.6	6.8 ± 1.5
4	2.9 ± 0.2	6.2 ± 2.8	2.1 ± 1.4	0.54 ± 0.4	6.8 ± 0.7	21 ± 6.7	2.4 ± 5.7

[a] All values calculated from 10 mg/kg po unless otherwise stated. [b] Half-life in (h). [c] Maximum exposure in (μM). [d] Time at maximum exposure (h). [e] Volume of distribution in L/kg (calculated from 1 mg/kg IV dose to mice). [f] Clearance in (mL/min/kg). Calculated from 1 mg/kg IV dose to mice ($n = 4$). [g] Exposure calculated as $t_0 \rightarrow$ infinity in (μM · h) following 10 mg/kg po dose to mice ($n = 5$). [h] Bioavailability calculated from 1 mg/kg IV dose and 10 mg/kg po dose. Compound **2** values calculated from $n = 3$ experiments (both 1 mg/kg IV and 10 mg/kg po). Compound **4** values determined from $n = 2$ experiments (both 1 mg/kg IV and 10 mg/kg po).

The enhanced pharmacology observed with **2** relative to **1** was observed despite a reduction in overall exposure. This observation indicated that the enhanced lymphopenia observed with **2** is likely a consequence of increased intrinsic potency against S1PL.

That oxime **2** generated substantial lymphopenia suggested the possibility that other analogues displaying a sp^2-hybridized heteroatom at this position might also provide potent analogues. We considered that heterocycles containing an appropriately oriented C=N bond within a heterocyclic ring could provide pharmacologically active compounds. To test this hypothesis, isoxazole **4**, the aromatic analogue of **2**, was orally administered to mice at 30 mg/kg and resulted in a dramatic reduction in circulating lymphocytes. Pharmacokinetic evaluation of **4** showed up to a 3-fold enhancement in exposure over oxime **2**. The more highly saturated dihydroisoxazole **5** showed less activity than the aromatic congener. Regioisomeric isoxazole **8** proved to be an inactive compound. Investigation into the effect of the isoxazole substitution revealed that addition of alkyl groups at the 5-position detracted from activity. As is apparent from methyl isoxazole **9**, cyclopropyl isoxazole **10**, isopropyl isoxazole **11**, and phenyl isoxazole **12**, potency generally decreased with increasing steric bulk vicinal to the isoxazole oxygen. Because this series of compounds displayed comparable levels of exposure, the effect on potency probably relates to a disfavored steric

Table 3. Pharmacokinetic Parameters of Compound **2** in Multiple Species

species[a]	D_{cse}[b]	T_{max}[c]	C_{max}[d]	AUC[e]	Vss[f]	CL[g]	%F[h]
rat	10	2.0	2.7	18.7	0.6	10.2	26.0
dog	50	2.0	79.5	323.0	0.3	3.5	32.1
monkey	30	2.3	16.9	70.1	0.5	4.8	16.4
human	~1	2.0	3	19.0			

[a] Male Sprague−Dawley rats; Beagle breed dogs; cynomolgous monkeys; healthy human volunteers. [b] Oral dose in mg/kg. [c] Time at maximum exposure (h). [d] Maximum exposure in (μM). [e] Exposure calculated as $t_0 \rightarrow$ infinity in (μM·h) following indicated dose. [f] Volume of distribution in L/kg. [g] Clearance in (mL/min/kg). Calculated from 1 mg/kg IV dose [h] Bioavailability calculated from 1 mg/kg IV dose and indicated oral dose.

interaction in this region. Introduction of electron withdrawing groups at the 5-position, as in trifluoromethyl isoxazole **13**, significantly reduced in vivo potency. Introduction of an electron donating group, as presented by ether **14**, also proved fruitless. Probing for a potential donor−acceptor interaction vicinal to the isoxazole heterocycle, alcohol **15** and amine **16** were also studied. In both cases, diminished activity suggested that no such interaction was realized.

While substitution at the 5-position of the pendant isoxazole heterocycle uniformly reduced potency, the effect of substitution at the 4-position was variable. Comparison of isoxazole **17** with isoxazole **9** indicates that the acetyl group reduces the degree of lymphopenia after oral dosing at 30 mg/kg. Nitro-arene **18** exhibited modest in vivo activity despite a slight decrease in exposure. 4-Substitued alkyl **19** triggered notable lymphopenia with good exposure. Electron withdrawing groups at the 4-position tended to reduce potency, while alkyl substitution was generally tolerated.

Owing to its superior in vivo activity following oral administration to mice, excellent solubility, and overall favorable physical properties, including pharmacokinetic properties, oxime **2** was further profiled. Following its discovery, isoxazole **4** was similarly profiled. Compounds **2** and **4** are both low molecular weight, polar compounds (MW 245, 255, respectively, PSA ~ 140, AlogP ~ −1.5), and their HCl salts were both easily formulated in neutral water. As shown in Table 2, a more detailed pharmacokinetic analysis revealed that both compounds show low clearance and a low volume of distribution. Additionally, they were characterized by a short half-life and quickly reached maximum concentrations in blood. Plasma concentrations of **2** and **4** were sufficiently sustained, and the AUC values were 8.8 μM·h and 21.0 μM·h, respectively, at 10 mg/kg oral dose. Owing to their PK/PD profile and performance against multiple animal models of arthritis (vide infra), compound **2** was nominated for clinical development. Subsequently, isoxazole **4** demonstrated outstanding properties and was nominated for clinical development as a backup compound to **2**.

To facilitate advancement of **2** to clinical evaluation, a more detailed pharmacokinetic profile was obtained in multiple species (Table 3). Compound **2** was characterized by low clearance and low volume of distribution following pharmacokinetic studies in rodents, dogs, monkeys, and, ultimately, humans. Maximum plasma concentrations occurred at approximately 2 h following oral administration. Exposure generally increased with higher species, showing the highest exposure in humans.

Pharmacodynamic Aspects of S1PL Inhibition. The PK-PD relationship for **1** demonstrated a significant time delay between oral administration of the compound and onset of
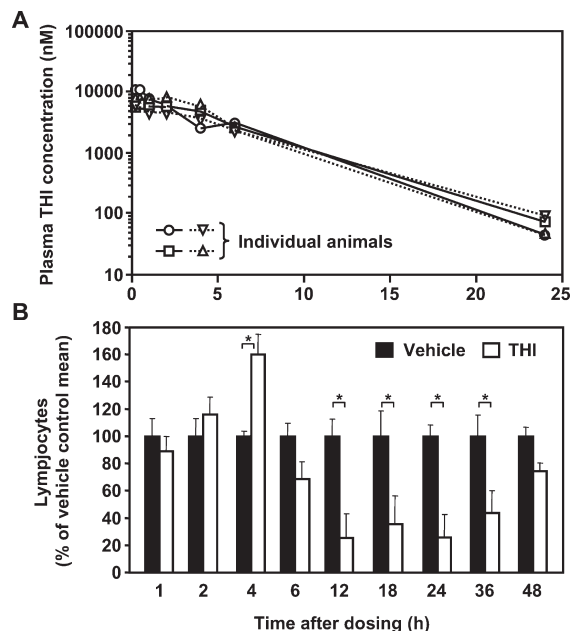
Figure 1. Pharmacokinetic and pharmacodynamic relationship of **1** in mice. (A) Pharmacokinetic analysis of **1** following 100 mg/kg PO dose to male C57BL/6 albino mice ($n = 4$). (B) Lymphocyte levels now normalized to vehicle control, *$p < 0.05$; single 100 mg/kg dose was given to mice ($n = 5$). Change in circulating peripheral lymphocytes is shown for mice treated with **1** at time points following oral gavage. Peak lymphopenia observed with **1** occurs over ten hours past peak plasma levels.

pharmacology, as assessed by reduced peripheral circulating lymphocyte numbers. The nadir in blood lymphocytes occurred 12−24 h following administration of **1**, following the peak plasma levels of **1** by more than 10 h (Figure 1).[8,12] Data for compounds **2** and **4** was in agreement with this observation. In fact, at the 18 h time point, when peripheral lymphopenia was at or near its maximum, **2** or **4** concentration in plasma was no longer detectable. Small polar molecules like **2** often achieve tissue concentrations by paracellular absorption.[13] Intracellular concentrations of drug are likely AUC driven, and the exposure achieved by in vivo administration is sufficient to inhibit S1PL activity in immune tissues that results in a gradual increase of S1P levels within these tissues.[8] Following prolonged S1PL inhibition, the increased S1P concentration (i.e., the S1P gradient) triggers receptor internalization which limits lymphocyte egress from secondary lymphoid tissue and therefore acts locally to lower levels of lymphocytes in peripheral circulation. In addition, the delayed pharmacodynamic effect of S1PL inhibition is consistent with both the intracellular location of S1PL and its slow turnover rate for S1P decomposition.[14] By contrast, administration of the direct S1PR agonists like FTY-720 leads to a more rapid onset of pharmacology.[15]

To determine the relationship between S1P tissue concentration and the pharmacodynamic profile of **2**, a comprehensive analysis of tissue S1P content and peripheral blood lymphocyte levels was performed in Sprague−Dawley rats (Figure 2). Consistent with our dosing protocol in mice, **2** (30 mg/kg) or vehicle was orally administered daily for 3 days and multiple tissues were assayed for S1P content 18 h after the final oral administration of **2**. The tissues included thymus, spleen, jejunum, lymph node, heart, eye, liver, kidney, and lung. CBC readings at 18 h taken immediately before tissue collection correlated with reduced levels of
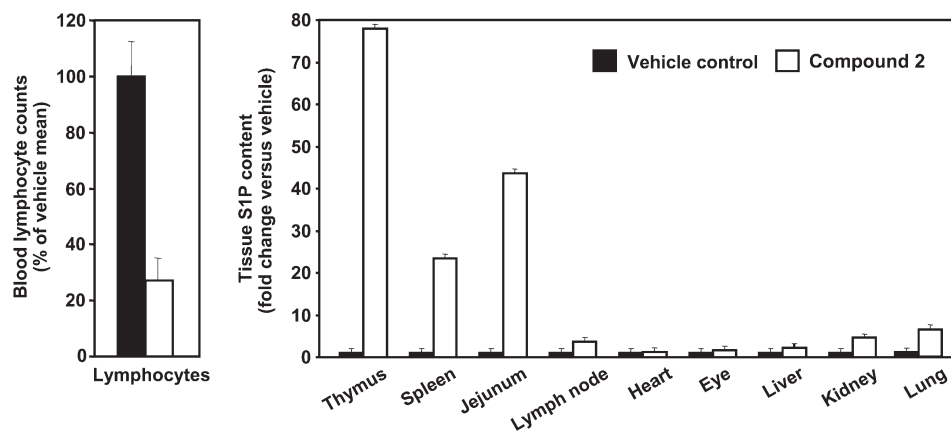
Figure 2. The lymphoid system is the primary target of compound **2** activity. Male Sprague−Dawley rats were treated with **2** or vehicle ($n = 10$ per tissue type, $n = 10$ for CBC). Group dosed orally with **2** at 30 mg/kg qd for 3 days. Blood and tissues were harvested 18 h after final dose. Blood lymphocyte counts were measured by CBC analysis.

peripheral circulating lymphocytes. The nadir of lymphopenia was concomitant with increased S1P concentration (Figure 2). S1P levels in thymus, spleen, and jejunum increased approximately 80-, 24-, and 45-fold, respectively, in rats treated with **2** over tissues from untreated rats. By contrast, several other nonlymphoid tissues, including the heart and eye, displayed no increase in S1P levels. Cardiac and ophthalmic tissues were of particular interest because adverse pharmacology is manifested in these tissues following administration of a S1PR agonist.[4] The observed tissue-selective increase in endogenous S1P resulting from S1PL inhibition distinguishes this target from synthetic S1P receptor agonists that have the capacity to modulate S1P receptors in a wide variety of tissues.[12] The lymphoid-tissue selective increase in S1P in response to S1PL inhibition is likely due to differential expression profiles of S1PL and other S1P regulating enzymes (i.e., sphingosine kinases, S1P phosphatase, S1P transporter) across the spectrum of tissue types.[21b] For example, while S1PL is widely expressed, S1P homeostasis in lymphoid tissues may be particularly sensitive to inhibition of S1PL activity due to reduced representation of mechanisms that decrease S1P levels. Furthermore, that a localized increase in S1P concentration does not lead to substantial increase in systemic S1P levels suggests that S1P exerts a relatively local effect primarily in lymphoid tissues.

Another mechanistic nuance in this signaling pathway relates to the relationship between **1** and S1PL. In accord with previous studies with **1**, compounds **2** and **4** showed no direct inhibition of S1PL when tested in our in vitro assay. To date, in vitro assay conditions required to determine direct S1PL inhibition by **1** or analogues thereof, remain elusive.[6,8] Previous mechanistic studies with **1** revealed that oral administration led to maximum lymphopenia (12−24 h after oral dose, measured in blood by CBC) and correlated with a concomitant decrease in S1PL activity and enhanced S1P levels in lymphoid tissue.[8] This suggests that the established in vivo efficacy is potentially due to a more complex scenario than a simple binary ligand−protein interaction and may result from a higher-order complex. Described here, mechanistic studies in rat with **2** showed enhanced S1P levels mainly in lymphoid tissue at peak lymphopenia (Figure 2). Accordingly, we performed comparative analysis of analogues of **1** *directly by in vivo analysis* using CBC measurements of peripheral lymphocyte levels at 18 h.

Direct in vivo evaluation of potential drug candidates is less common to the current drug discovery paradigm that has most heavily relied on in vitro methods during the last two decades. However, direct in vivo testing has been of tremendous benefit to the drug discovery process historically, from aspirin[16] and penicillin[17] to the development of modern imaging and X-ray contrast agents.[18] A more recent example of in vivo screening methods in modern drug discovery can be found in the S1P signaling pathway itself. In 1995, Adachi and co-workers[19] applied ex vivo and in vivo screening tools to the SAR of myriocin,[20] a serine palmitoyltransferase inhibitor with potent immunosuppressant activity.[21] Continued in vivo screening of analogues, without application of an in vitro screening tool, led to the discovery of FTY720 (fingolimod).[22] Interestingly, in vitro analysis of this analog revealed no inhibition of serine palmitoyltransferase. Subsequently, it was discovered that in vivo phosphorylation of fingolimod was necessary for its immunosuppressant activity. Ultimately it was determined that phosphorylated fingolimod is a direct S1P receptor agonist. Since myriocin and fingolimod act on different biological targets, in vitro screening alone could not have predicted the striking in vivo potency of fingolimod. Oral administration of these analogs, in vivo pharmacology experiments, and ex vivo analysis of blood samples by CBC were therefore crucial to the discovery of fingolimod.

Pharmacology. Mice with reduced levels of S1PL activity due to genetic modification or treatment with **1** present an altered pattern of lymphocyte trafficking and changes in tissue S1P concentration,[1a] analogous to manipulation of the S1P/S1PR axis by fingolimod.[23] Importantly, the physiological effects of inhibiting S1PL activity by more than 90% is limited to the immune system.[1] Oral dosing with **2** or **4** recapitulated the changes in lymphocyte trafficking and tissue S1P concentrations observed in genetically modified mice expressing reduced levels of S1PL activity. These results suggested that immune modulation achieved by treatment with compounds **2** or **4** may be of therapeutic benefit in inflammatory and autoimmune diseases. Dose escalation studies indicated that single oral doses of 30−100 mg/kg **2** administered to mice induced 40−60% lymphopenia, while lower doses have a minimal to nonstatistically significant effect (Figure 3).

The effect of **2** and **4** on disease development and progression was assessed in a collagen-induced arthritis (CIA) model of rheumatoid arthritis (RA) in mice, using prophylactic and therapeutic dosing regimes. In vivo models of collagen-induced arthritis using prophylactic dosing of 100 mg/kg **2** resulted in a significant delay in the onset of arthritis; treated
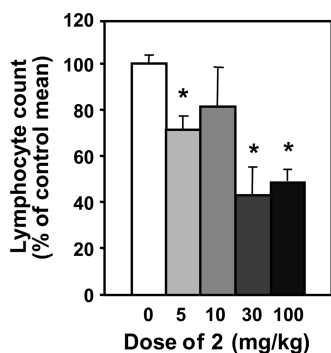
Figure 3. Compound **2** treatment induces up to 60% depletion of circulating lymphocytes. Mice were treated with the indicated single oral doses of **2**, and blood lymphocyte counts were measured 18 h after dosing. Data were pooled from three independent experiments, giving similar results and represent 8−10 mice each cohort. Data are presented as mean ± SEM; *$p < 0.05$.

mice had only a minimal increase in clinical scores and joint swelling (Figure 4A). As expected from its effect on T-cell trafficking, mice treated with **2** showed an approximately 40−60% decrease in the number of circulating T cells and an increased percentage of CD4 and CD8 single positive cells in the thymus at the conclusion of the experiment (Figure 4B). Microscopic analysis of tarsal sections showed that treatment with **2** significantly reduced synovial hyperplasia, inflammation, erosion, and exudate formation (Figure 4C). Statistical analysis of histopathology scores confirmed that treatment with **2** effectively reduced joint damage, hyperplasia, and immune cell infiltration compared to vehicle control.

The effect of **2** and **4** was further assessed in CIA using a therapeutic dosing regime whereby **2**, **4**, or vehicle control was administered once 50% of the animals within the group became symptomatic. Using this dosing paradigm, both **2** and **4** dosed at 30 mg/kg gave significant relief from disease as measured by clinical scores and joint swelling, compared to vehicle control (Figure 5A). Therapeutic treatment with **2** or **4** at a dose which induces minimal lymphopenia (5 mg/kg, Figure 3) also yielded a trend of reduced disease activity (Figure 5A).

The disease-modifying efficacy observed in the presence of relatively mild lymphopenia during both prophylactic and therapeutic treatments indicates that the potent anti-inflammatory effect of S1PL inhibition cannot be explained solely by the effect on the levels of circulating lymphocytes. It is important to note that a 40% decrease in circulating lymphocyte numbers alone is not expected to affect mouse inflammatory challenge models. Several other gene knockout lines have been analyzed at Lexicon that exhibited significant lymphopenia without resistance to inflammatory challenge (data not shown). While alteration of lymphocyte trafficking likely plays a significant role in immunosuppression via S1PL inhibition, the increased S1P levels may also affect other biological processes, in addition to cell migration, contributing to the observed anti-inflammatory effect. These processes may include the inflammatory response of cell types as diverse as endothelial cells,[24] macrophages,[25] and NK cells.[26] Importantly, the disease-modifying effect of **2** and **4** was not due to general immunosuppression because the antibody responses to the injected CII antigen were not blocked by treatment with compound (Figure 5B). Taken together, the results suggest that inhibition of S1PL activity can achieve significant anti-inflammatory effect without hampering the immune response completely. Of note, the
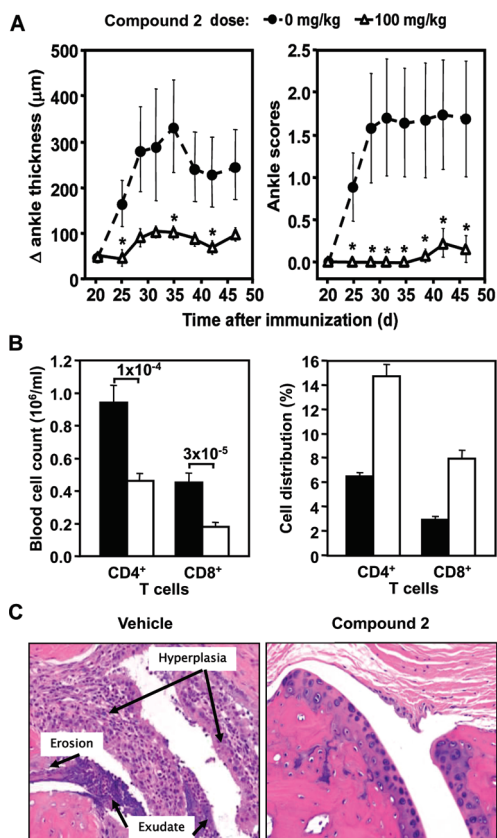

Figure 4. Compound **2** prevents arthritis development in the mouse collagen-induced arthritis model. (A) Average values for clinical scores (left panel) and joint swelling (right panel) taken from the hind limbs for vehicle control ($n = 16$) and compound **2** ($n = 13$) arms are shown with vertical bars representing SEM. *X* axis values represent days after collagen immunization. Daily oral dosing was initiated on day −1; the vehicle control mice were given 10 mL/kg water, and the compound **2** cohort was given 100 mg/kg compound in 10 mL/kg water. *$p < 0.05$. (B) Analysis of CD4 and CD8 single positive T cells in blood and thymus as indicated. Bars represent average values, black for vehicle control, and white for **2**; SEM is indicated by the vertical lines. Blood data were obtained from 13−16 animals per cohort; two animals per arm were used for thymus staining; numbers above bars indicate *p* values. (C) H&E staining of representative tarsal joint sections from control (left) and **2** treated (right) animals shown at 10× magnification. Regions of synovial hyperplasia, inflammation, and erosion are highlighted by small arrows (minimal in **2** sample).

murine CIA results were further supported by analysis of efficacy of compounds **2** and **4** in the rat adjuvant-induced model of RA, a particularly aggressive model of RA.[27]

Telemetry Studies. Given that bradycardia was a clinical observation associated with fingolimod,[4a] the effect of **2** administration on heart rate was assessed in multiple species. Assessment of cardiovascular effects of **2** in dogs and primates was based on measurements of electrocardiogram (ECG) and hemodynamic parameters (blood pressure and heart rate). Cynomolgus monkeys and dogs were administered single ascending doses up to 1000 mg/kg and 500 mg/kg, respectively. Compound **2** did not affect heart rate at the highest dose studied, in either dog or in primate (Figure 6). These data correlate with the observation that inhibition of S1PL affects S1P concentration primarily in lymphatic tissues.

Phase I Clinical Trial Data for Compound 2. On the basis of the preclinical data demonstrating a favorable safety
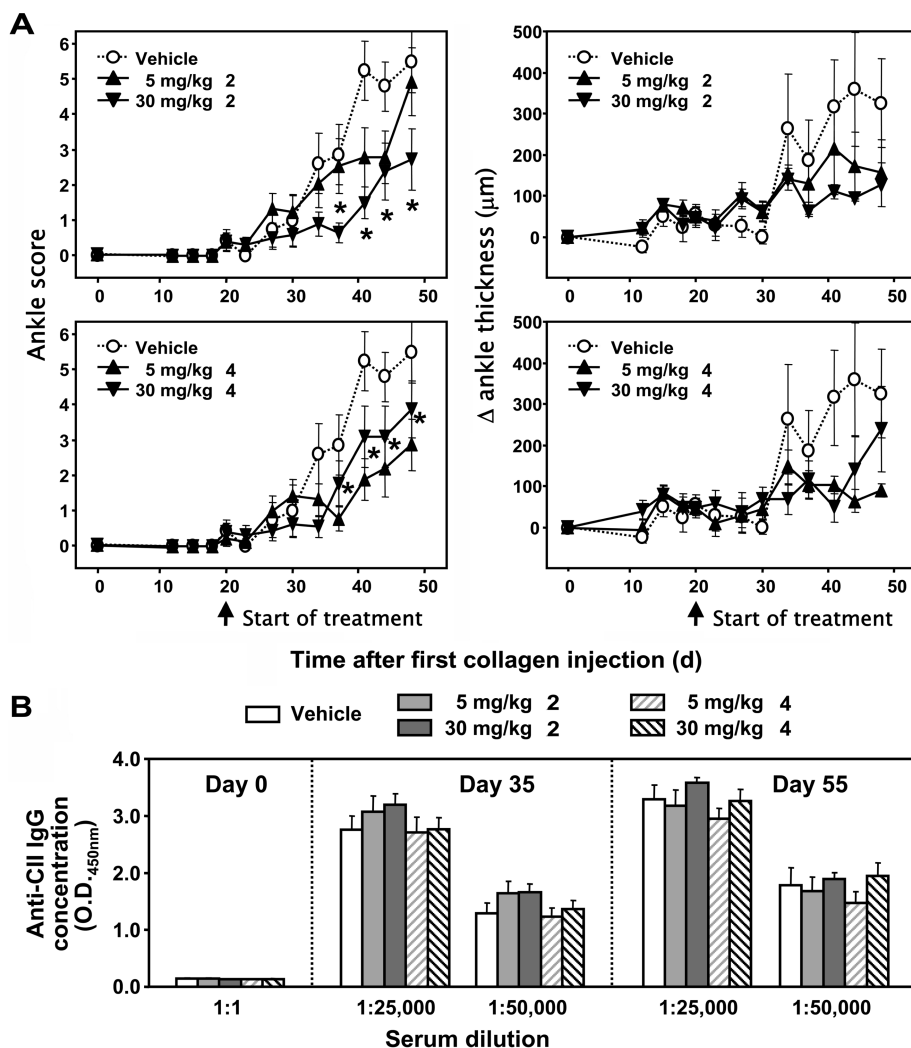
Figure 5. Therapeutic dosing of **2** and **4** reduces severity of cia symptoms in mice. (A) Average values for joint swelling (left panel) and clinical scores (right panel) taken from the hind limbs for vehicle control (circles) and **2** (triangles) arms are shown with vertical bars representing SEM. *X*-axis represent days after collagen immunization. Daily oral dosing was initiated on day 20 (arrow), Vehicle control mice were given 10 mL/kg water; **2** was given at the indicated doses po in 10 mL/kg water. $n = 9-10$ each cohort; *P value < 0.05. (B) Serum anti-CII Ab titers of mice from the study presented in (A) were measured by ELISA at the indicated time points after initial collagen immunization.
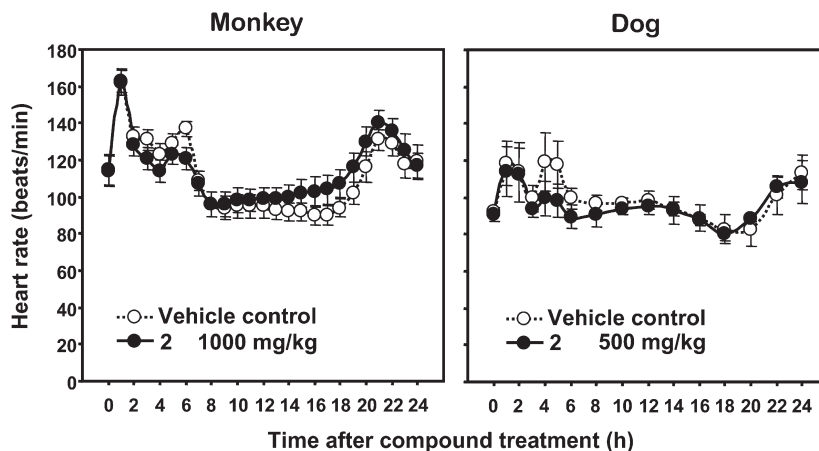
Figure 6. Telemetry studies of compound **2** in primate and dog. Ten male Cynomolgus monkeys (*Macaca fascicularis*) were given a single administration of 1000 mg/kg using a Latin square design by oral gavage. Electrocardiogram (ECG), blood pressure, and heart rate were used to monitor cardiovascular and hemodynamic parameters. Telemetry data collection began 90 min prior to dosing and continued at the indicated time points for 24 h. Four female Beagle dogs were given a single dose administration of 500 mg/kg using a Latin square design by oral gavage. Data collection commenced 24 h prior to dose administration. One-minute tracings of ECGs were obtained at approximately 15 min prior to dosing and at time intervals shown.
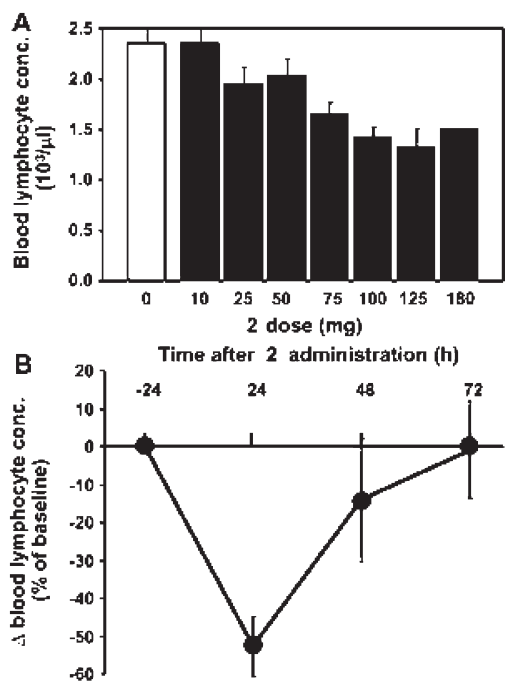
Figure 7. Phase 1a clinical trial data: lymphocyte counts are decreased after treatment with compound **2**, with recovery 48 h after nadir. (A) Dose-dependent reduction in lymphocyte counts observed after single dose phase 1a trial: 159 patients total in single and multiple ascending dose studies; 120 active dosing regimens and 39 placebo regimens, participated in randomized, double-blinded study. (B) Rapid reduction of blood lymphocytes from a single 125 mg dose ($N = 6$ patients) followed by a return to baseline in 48 h after nadir.

and efficacy profile of LX2931, phase 1 clinical trials were initiated to determine safety in human subjects. As a surrogate biomarker of S1PL inhibition, blood lymphocyte populations were determined by CBC analysis. As shown in Figure 7A, a single ascending dose provided a clear dose-responsive relationship, resulting in up to a ~50% decrease in peripheral lymphocytes at the highest administered dose of 180 mg. The compound was generally well tolerated in all dose groups. Importantly, the induced reduction in circulating blood lymphocytes ($N = 6$, 125 mg single dose) was reversible (Figure 7B); lymphocyte populations rebounded to predose levels by 48 h after nadir.

Conclusion

S1PL appears to play a more significant role in controlling the S1P gradient in lymphoid tissues than in other tissues. This local effect has the systemic impact of lowering levels of lymphocytes in peripheral circulation. Increased S1P levels after inhibition of S1PL may also affect secondary mechanisms that contribute to anti-inflammatory activity. Exploration of the SAR of **1** and identification of the pendant 2-acetyl group was crucial to the discovery of **2**. Recognition of the importance of the oxime was the basis for the rational design of the isosteric isoxazole contained within **4**. Compound **2** has shown robust efficacy in multiple disease models of rheumatoid arthritis. Peripheral lymphocyte levels have been similarly reduced by oral administration of **2** across multiple species studied, from mouse to man. Phase II trials are currently underway in patients with active rheumatoid arthritis. Results on these studies will be reported as they become available.

Experimental Procedures

Animal Handling and in Vivo Methods. All procedures were conducted according to applicable standard operating procedures and with the approval of the Lexicon Pharmaceuticals, Inc. Institutional Animal Care and Usage Committee. For PK analysis, the tested analogues were formulated in sterile water and dosed to 129/SvEvBrd × C57BL/6 F1 mice. The pH of intravenous dosing solution was adjusted to between 5 and 6 and between 3 and 4 for oral administration. The intravenous dose volume was 3.7 mL/kg body weight, and the oral gavage volume was 5 mL/kg body weight at 1 and 10 mg/kg body weight, respectively. Animals were observed regularly throughout the day on days in which they were dosed, and these clinical observations were recorded. For the purpose of exposure, blood was collected using saphenous vein bleeds in unanaesthetized animals, except for terminal bleeds, which were performed using cardiac puncture immediately following euthanasia. Blood samples were collected at 0.08, 0.25, 0.5, 1, 3, and 6 h post intravenous dosing and at 0.25, 0.5, 1, 2, 4, 6, and 24 h post oral administrations. An aliquot of 25 μL of blood in K_2-EDTA tubes was spun following each time point, and 10 μL of the resulting plasma was transferred to fresh polypropylene tubes for exposure assessment by liquid chromatography−mass spectrometry according to the following experimental LC/MS protocol: Compound **2** levels in plasma were determined using a Thermo Finnigan TSQ Quantum Ultra AM, Thermo Finnigan Sureyor MS LC Pump, and CTC Analytics HTC PAL autosampler. A Phenomenex Luna phenyl-hexyl, 4.6 mm ×50 mm column was used for chromatography. The mobile phases used in the gradient chromatography method were: A, water with 0.1% formic acid; B, acetonitrile with 0.1% formic acid. The gradient had the following time profile: 0 min, 95%A; 0.5 min, 95% A; 1 min, 5%A; 2.5 min, 5%A; 2.51 min, 95%A; 3 min, 95%A. The chromatographic flow rate was 0.7 mL/min and the injection volume was 15 μL. Positive ion ESI LC/MS/MS analysis was used for detection of the analyte. The multiple reaction monitoring transition for **2** detection was 246 → 210 m/z, collision energy was 14 eV, and the tube lens energy was 77 V. Determination of sphingosine 1-phosphate levels were made according to protocol published in detail in the supporting online material by Schwab and Cyster.[6]

Cardiovascular Evaluation of 2: Administration by Oral Gavage to Telemetry-Instrumented Conscious Nonhuman Primate. Ten male Cynomolgus monkeys (*Macaca fascicularis*) were assigned to study and given a single oral administration of **2** dosages using a Latin square design. Assessment of cardiovascular effects was based on measurements of electrocardiogram (ECG) and hemodynamic parameters (blood pressure and heart rate). The general health of the animals was assessed based on body weights, clinical signs, and intra-abdominal body temperature. Telemetry data were collected for at least 90 min prior to dosing and continuously for at least 24 h postdose. Quantitative ECG analysis was completed for baseline and at time intervals post dose indicated in Figure 6.

Cardiovascular Effects of 2 Administered to Conscious Telemetered Dogs. Four female Beagle dogs were assigned to study and given a single administration of all dosages using a Latin square design. Animals were administered various single doses and dosed via oral gavages. The data collection commenced approximately 24 h prior to dose administration and continued for approximately 24 h post dose. Data was collected continuously. One-minute tracings of the ECGs were obtained at approximately 15 min prior to dosing and at intervals indicated in Figure 6.

Collagen-Induced Arthritis. For experiments utilizing prophylactic dosing of test compounds a synovial autoimmune response was induced in 129/SvEvBrd × C57BL/6 F1 mice as previously described.[28] Studies utilizing the therapeutic dosing regime were performed using DBA1/j mice and CFA containing a reduced concentration of *Mycobacterium tuberculosis* (4 mg/mL).

Detection of Anti Type II Collagen (CII) Antibodies. Total CII-specific IgG antibody levels were determined in preimmunization and day 35 sera by ELISA. Briefly, 96-well Nunc Maxisorp flat-bottomed plates (Fisher, Pittsburgh, PA) were coated with 100 μL/well of 2 μg/mL chicken collagen II (Sigma, St Louis, MO) in PBS and incubated overnight at 4 °C. Plates were subsequently washed four times with 100 μL of PBS/Tween per well and then blocked for 1 h with 100 μL of PBS containing 10% FBS. Then 100 μL of a 1:25000 dilution of sera was loaded into wells and incubated for 1 h at room temperature. Wells were washed as before and 100 μL of a 1:5000 dilution of horseradish peroxidase-conjugated goat antimouse total IgG (H+L) (Southern Biotech, Birmingham, AL) was added to each well and incubated at RT for an hour. Plates were washed a final time and peroxidase activity was assessed using the 3,3',5,5'-tetramethylbenzidine (TMB) liquid substrate system for ELISA per manufacturer's instructions (Sigma, St Louis, MO). OD_{450} was determined using a Vmax kinetic microplate reader (Molecular Devices, Sunnyvale, CA). The concentration of CII-specific antibody was expressed as the OD_{450} of the sample minus the OD_{450} of the blank.

Chemical Methods. All reactions were conducted under a static atmosphere of argon or nitrogen and stirred magnetically unless otherwise noted. Reagents, starting materials, and solvents were purchased from commercial suppliers and used as received. Flash column chromatography was carried out using prepacked silica gel columns from Biotage or ISCO or by slurry preparation using EMD Silica Gel 60 (particle size 0.040–0.063 mm). ^{1}H and ^{13}C NMR spectra were collected on Bruker ARX300, DRX400, or DPX400, or Varian Mercury 400 MHz NMR spectrometers. Chemical shifts are reported in parts per million (ppm) relative to tetramethylsilane in δ-units, and coupling constants (*J*-values) are given in hertz (Hz). Data are reported in the following format: chemical shift, multiplicity, coupling constants, and assignment. Reactions were monitored by TLC using 0.25 mm E. Merck silica gel plates (60 F_{254}) and were visualized with UV light. Analytical HPLC spectra were collected on Shimadzu HPLC systems equipped with a UV detector measuring absorbance at 220 and 254 nm. Purity was determined to be ≥95% purity for all compounds contained within this manuscript using a Shimadzu analytical HPLC by the method specified in the experimental procedure. Mass spectra were obtained on Waters ZQ or ZMD LCMS systems equipped with an autosampler, and ELSD detector, a UV detector measuring absorbance at 220 and 254 nm, and a mass detector. High resolution mass spectra were obtained on a Waters LCT Premier XE Micromass MS Technologies instrument equipped with an autosampler. Elemental analysis was conducted by Robertson Microlit Laboratory, Madison, NJ.

(*E*)-1-(4-((1*R*,2*S*,3*R*)-1,2,3,4-Tetrahydroxybutyl)-1*H*-imidazol-2-yl)ethanone Oxime (2). To a flask charged with 1 (4.88 g, 21.20 mmol) was added water (25 mL) and 1 N aqueous HCl (21.2 mL, 21.2 mmol). After all solids dissolved, a solution of trityl hydroxylamine (7.00 g, 25.44 mmol) in dioxane (55 mL) was added and the reaction was maintained at 50 °C for 4 h. At completion, the reaction was cooled to room temperature and the solution was adjusted to pH = 7 by addition of 1N aqueous NaOH . The neutralized solution was then concentrated to a plastic mass, which was purified by flash chromatography on silica gel [10% MeOH/1% NH$_4$OH (5 wt % solution in water) in DCM] to provide the trityl-ether as clear plastic. The plastic mass was azeotroped with hexane and concentration provided a white foam, which could be dried under vacuum to a solid.

To a vigorously stirred, room temperature solution of the obtained intermediate trityl oxime-ether (4.8 g, 10 mmol) in dioxane (90 mL) was added a solution of HCl in dioxane (4.0 M, 60 mL). After a few minutes, a white precipitant was observed, and stirring was continued for a total of 30 min before filtering over a fritted glass filter and rinsing the cake with dioxane and ether. The cake was redissolved in water (200 mL), sonicated for

5 min then cooled to 0 °C, treated with Celite (5 g) and filtered over a fritted glass filter. The aqueous solution was concentrated to dryness then triturated with methanol:diethyl ether (30 mL: 60 mL) to provide the *E*-oxime as an analytically pure white powder (3.8 g, 79% yield, 2 steps). ^{1}H NMR (400 MHz, 1 M DCl in D$_2$O) δ 7.47 (d, *J* = 0.50 Hz, 1 H), 5.20 (dd, *J* = 2.26 Hz, 0.75, 1H), 3.85 (dd, *J* = 13.05, 2.76 Hz, 1H), 3.82 (dd, *J* = 13.05, 2.51 Hz, 1H), 3.76 (dd, *J* = 8.53, 2.26 Hz, 1H), 3.65−3.72 (m, 1 H) 2.30 (s, 3H). ^{13}C NMR (101 MHz, 1.0 M DCl in D$_2$O) δ146.85, 144.03, 138.02, 119.94, 75.59, 73.60, 67.49, 65.77, 13.5. MS (EI) *m/z*: 246 [M + H]$^{+}$. HRMS calcd for C$_9$H$_{15}$N$_3$O$_5$ [MH]$^{+}$ 246.1090, found 246.1082; mp 101 °C. HPLC (Zorbax 4.6 mm × 150 mm, 2−40% [methanol/water/TFA (95/5/0.1)]: water, 6 min gradient) t_R = 1.15 min, 100% integrated area.

(1*R*,2*S*,3*R*)-1-(2-(Isoxazol-3-yl)-1*H*-imidazol-4-yl)butane-1,2,3,4-tetraol (4). A solution of trityl hydroxylamine (15.15 g, 55 mmol) in dioxane (120 mL) was added to a solution of 1-HCl (13.30 g, 50 mmol) in water (60 mL), and the reaction was maintained at room temperature with vigorous stirring for 4 h. At completion, the reaction was quenched with excess triethylamine (10 mL) and then concentrated and flashed over silica gel (5−10% MeOH/DCM) to provide an intermediate plastic mass that was azeotroped with toluene (2 × 200 mL). The plastic mass was redissolved in 1,1-dichloroethane (250 mL) and 2,2-dimethoxypropane (250 mL) and then treated with *p*-TsOH-H$_2$O (1.28 g, 7.72 mmol) and heated to 60 °C for 16 h. At completion, the reaction was diluted with dichloromethane (500 mL) and washed with satd aq NaHCO$_3$ (2 × 200 mL), water (200 mL), and brine (200 mL) and then dried over MgSO$_4$ and concentrated. The resulting plastic mass was azeotroped with toluene (200 mL) and then redissolved in anhydrous dioxane (300 mL) and treated with 4 N HCl (150 mL) in anhydrous dioxane. After maintaining at room temperature for 1 h, the reaction was concentrated, then flashed over silica gel (3−10% MeOH: DCM eluent) to provide 2 (7.87 g, 48% yield, 3 steps).

A solution of 2 (1.65 g, 5.08 mmol) in THF (50 mL) was cooled to −15 °C and then treated with a 1.6 M solution of *n*-BuLi in hexanes (18.5 mL, 29.60 mmol). The reaction was maintained for 30 min and then quenched with anhydrous DMF (3.92 mL, 50.8 mmol). The reaction was allowed to warm to room temperature for 30 min and then quenched with satd aq NH$_4$Cl (50 mL) and diluted with EtOAc (200 mL). The layers were separated, and the organics were washed with water (100 mL) and then brine (50 mL) before drying over MgSO$_4$ and concentrating. The resulting crude material was purified by flash chromatography over silica gel (3−8% MeOH/DCM eluent) to provide a plastic mass (1.10 g, 3.12 mmol). The material was redissolved in THF (10 mL) and then cooled to 0 °C and treated sequentially with pyridine (0.95 mL, 12.48 mmol) and trifluoroacetic acid anhydride (0.52 mL, 3.74 mmol). The reaction was then warmed to 50 °C for 16 h and then concentrated and flashed over silica gel (5−8% EtOAc:hexanes eluent). The resulting material was dissolved in dioxane (10 mL) and treated with 1 M aq HCl and heated to 50 °C for 2 h, then concentrated. The solid was dissolved in water (10 mL) and then lyophilized to provide 4 as a white powder (321 mg, 22% yield, 3 steps). ^{1}H NMR (400 MHz, 1.0 M DCl in D$_2$O) δ 8.70 (d, *J* = 1.8 Hz, 1 H), 7.41 (s, 1 H), 6.88 (d, *J* = 1.5 Hz, 1 H), 5.07 (s, 1 H), 3.72−3.43 (m, 4 H). ^{13}C NMR (101 MHz, 1.0 M DCl in D$_2$O) δ ppm 162.23, 148.64, 136.24, 133.98, 117.83, 103.47, 72.59, 70.51, 64.48, 62.73. MS (EI) *m/z*: 256 [M + H]$^{+}$. HRMS calcd for C$_{10}$H$_{13}$N$_3$O$_4$S [M + H]$^{+}$ 256.0933, found 256.0919. HPLC (Zorbax C8 4.6 mm × 150 mm, 5% [methanol/water/TFA (95/5/0.1)]:water, 5 min isocratic) t_R = 1.04 min, 100% integrated area.

General Procedure A: (1*R*,2*S*,3*R*)-1-(2-(Isoxazol-3-yl)-1*H*-imidazol-4-yl)butane-1,2,3,4-tetraol (4). To a room temperature solution of the nitrile[29] (80.0 g, 850 mmol) in MeOH (1700 mL) was added MeONa solution in MeOH (25% w/w, 110 mL, 510 mmol). After 1 h, the imidate formation was deemed complete

by ^{1}H NMR analysis of a reaction aliquot in MeOH-d_4. At this time, fructosamine−HOAc (202.4 g, 850 mmol) was added to the reaction in one portion. After 18 h, another portion of MeONa solution in MeOH (25% w/w, 92.0 mL, 425 mmol) was added to the heterogeneous reaction mixture. The reaction was maintained at room temperature with vigorous stirring for 24 h, then diluted with water (500 mL) and acidified to pH = 2 with conc aq HCl. The reaction was concentrated and then redissolved in water (800 mL) before adjusting to pH = 10 with 10 M aq NaOH. The precipitate was collected by filtration and rinsed with water. The precipitate was acidified with water and conc HCl to pH∼3, and then the freely soluble solution was concentrated to dryness. The resulting solid was azeotroped with toluene (2 × 1 L) to remove trace water. The solid was ∼98% pure at this stage but was purified further by dissolving in a minimum volume of hot MeOH and then crystallized after addition of diethyl ether and cooling. Filtration and drying on high vacuum afforded the HCl salt of **4** as a white crystalline powder (240 g, 97% yield). All analytical data was identical with the material generated by the initial medicinal chemistry route.

(1R,2S,3R)-1-(2-(5-Phenylisoxazol-3-yl)-1H-imidazol-4-yl)-butane-1,2,3,4-tetraol (12). Prepared according to the general procedure A from 5-phenylisoxazole-3-carbonitrile (170 mg, 1.00 mmol) and fructosamine−HOAc (238 mg, 1.00 mmol) to provide **12** as the HCl salt (327 mg, 89% yield). ^{1}H NMR (300 MHz, 1.0 M DCl in D$_2$O) δ ppm 7.74−7.83 (m, 2 H), 7.49 (s, 1 H), 7.39−7.46 (m, 3 H), 7.15 (s, 1 H), 5.12−5.17 (m, 1 H), 3.55−3.79 (m, 4 H). MS (EI) *m/z*: 332 [M + H]$^+$. HRMS calcd for C$_{16}$H$_{17}$N$_3$O$_5$ [M + H]$^+$ 332.1246, found 332.1259. HPLC (Zorbax 4.6 mm × 150 mm, 10−90% [methanol/water/TFA (95/5/0.1)]:water, 6 min gradient) t_R = 4.30 min, 98% integrated area.

(1R,2S,3R)-1-(2-(3-Methylisoxazol-5-yl)-1H-imidazol-4-yl)-butane-1,2,3,4-tetraol (8). Prepared according to the general procedure A from 3-methylisoxazole-5-carbonitrile (324 mg, 3.00 mmol) and fructosamine−HOAc (714 mg, 3.00 mmol) to provide **8** as the HCl salt (610 mg, 66% yield). ^{1}H NMR (400 MHz, 1.0 M DCl in D$_2$O) δ ppm 7.38 (d, J = 1.0 Hz, 1 H), 6.86 (s, 1 H), 5.04 (dd, J = 2.0, 0.8 Hz, 1 H), 3.52−3.66 (m, 3 H), 3.42−3.50 (m, 1 H), 2.16 (s, 3 H). ^{13}C NMR (101 MHz, 1.0 M DCl in D$_2$O) δ ppm 162.25, 153.36, 136.28, 132.20, 117.85, 107.89, 72.62, 70.52, 64.49, 62.73, 10.36. MS (EI) *m/z*: 270 [M + H]$^+$. HRMS calcd for C$_{11}$H$_{15}$N$_3$O$_5$ [M + H]$^+$ 270.1090, found 270.1081. HPLC (Luna Phenyl-hexyl 4.6 mm × 50 mm, 5% [10 mmol aq NH$_4$OAc:MeCN, isocratic) t_R = 0.73 min, 100% integrated area.

1-(5-Methyl-3-(4-((1R,2S,3R)-1,2,3,4-tetrahydroxybutyl)-1H-imidazol-2-yl)isoxazol-4-yl)ethanone (17). Prepared according to the general procedure A from 4-acetyl-5-methylisoxazole-3-carbonitrile (410 mg, 3.01 mmol) and fructosamine−HOAc (720 g, 3.01 mmol) to provide **17** as the HCl salt (81 mg, 23% yield). ^{1}H NMR (400 MHz, 1.0 M DCl in D$_2$O) δ ppm 7.57 (d, J = 0.5 Hz, 1 H), 5.21 (d, J = 1.3 Hz, 1 H), 3.74−3.82 (m, 2 H), 3.72 (d, J = 1.8 Hz, 1 H), 3.57−3.66 (m, 1 H), 2.83 (s, 3 H), 2.58 (s, 3 H). MS (EI) *m/z*: 312 [M + H]$^+$. HRMS calcd for C$_{13}$H$_{18}$N$_3$O$_6$ [M + H]$^+$ 312.1196, found 312.1181. HPLC (Sunfire C18 4.6 mm × 50 mm, 5% [methanol/water/TFA (95/5/0.1)]:water, 8 min isocratic) t_R = 3.03 min, 100% integrated area.

(1R,2S,3R)-1-(2-(5-Methylisoxazol-3-yl)-1H-imidazol-4-yl)-butane-1,2,3,4-tetraol (9). Prepared according to the general procedure A from 5-methylisoxazole-3-carbonitrile (216 mg, 2.0 mmol) and fructosamine−HOAc (476 mg, 2.0 mmol) to provide **9** as the HCl salt (403 mg, 75% yield). ^{1}H NMR (400 MHz, 1.0 M DCl in D$_2$O) δ ppm 7.54 (s, 1 H), 6.69 (s, 1 H), 5.20 (d, J = 1.0 Hz, 1 H), 3.69−3.86 (m, 3 H), 3.56−3.69 (m, 1 H), 2.49 (s, 3 H). ^{13}C NMR (100 MHz, 1.0 M DCl in D$_2$O) δ ppm 174.29, 150.01, 136.55, 134.96, 118.13, 100.98, 73.11, 71.01, 65.00, 63.20, 11.91. MS (EI) *m/z*: 270 [M + H]$^+$. HRMS calcd for C$_{11}$H$_{16}$N$_3$O$_5$ [M + H]$^+$ 270.1090, found 270.1108. HPLC (HILIC Silica 4.6 mm × 50 mm, 100−40% [methanol/water/TFA (95/5/0.1)]:water with 0.1% TFA, 3 min gradient) t_R = 0.30 min, 100% integrated area.

(1R,2S,3R)-1-(2-(5-(Trifluoromethyl)isoxazol-3-yl)-1H-imidazol-4-yl)butane-1,2,3,4-tetraol (13). Prepared according to the general procedure A from 5-(trifluoromethyl)isoxazole-3-carbonitrile (405 mg, 2.5 mmol) and fructosamine−HOAc (595 mg, 2.5 mmol) to provide **13** as the HCl salt (718 mg, 80% yield). ^{1}H NMR (300 MHz, 1.0 M DCl in D$_2$O) δ ppm 7.47 (d, J = 0.8 Hz, 1 H), 7.45 (d, J = 0.8 Hz, 1 H), 5.09 (d, J = 1.0 Hz, 1 H), 3.67−3.76 (m, 3 H), 3.52−3.60 (m, 1 H). MS (EI) *m/z*: 324 [M + H]$^+$. HRMS calcd for C$_{11}$H$_{13}$F$_3$N$_3$O$_5$ [M + H]$^+$ 324.0807, found 324.0815. HPLC (Sunfire C18 4.6 mm × 50 mm, 6−30% [methanol/water/TFA (95/5/0.1)]:water with 0.1% TFA, 5 min gradient) t_R = 1.07 min, 100% integrated area.

(1R,2S,3R)-1-(2-(5-Isopropylisoxazol-3-yl)-1H-imidazol-4-yl)-butane-1,2,3,4-tetraol (11). Prepared according to the general procedure A from 5-isopropylisoxazole-3-carbonitrile (489 mg, 3.57 mmol) and fructosamine−HOAc (850 mg, 3.57 mmol) to provide **11** as the HCl salt (1.03 g, 87% yield). ^{1}H NMR (400 MHz, 1.0 M DCl in D$_2$O) δ ppm 7.00 (d, J = 0.5 Hz, 1 H), 6.17 (d, J = 1.0 Hz, 1 H), 4.67 (dd, J = 1.9, 0.9 Hz, 1 H), 3.16−3.31 (m, 3 H), 3.04−3.14 (m, 1 H), 2.51−2.68 (m, 1 H), 0.67−0.77 (m, 6 H). MS (EI) *m/z*: 298 [M + H]$^+$. HRMS calcd for C$_{13}$H$_{19}$N$_3$O$_5$ [M + H]$^+$ 298.1403, found 298.1410. HPLC (Sunfire C18 4.6 mm × 50 mm, 10−90% 10 mM aq NH$_4$OAc:MeCN, 2 min gradient) t_R = 1.47 min, 97% integrated area.

(1R,2S,3R)-1-(2-(4,5-Dihydroisoxazol-3-yl)-1H-imidazol-4-yl)-butane-1,2,3,4-tetraol (5). To a −78 °C solution of the oxime **2** (2.40 g, 7.37 mmol) in THF (100 mL) was added a 1.6 M solution of *n*-BuLi in hexanes (27.6 mL, 44.2 mmol). The reaction was maintained at −78 °C for 15 min and then treated with DMF (4.5 mL, 59.0 mmol) and warmed to room temperature. After 2 h, the reaction was quenched with satd aq NH$_4$Cl solution (50 mL), then diluted with EtOAc (200 mL). The layers were separated and the organics were washed with water (100 mL) and brine (50 mL), dried over MgSO$_4$, and concentrated under vacuum to provide a white solid (1.63 g) which was redissolved in MeOH (45 mL). The solution was cooled to 0 °C and then treated portionwise with NaBH$_4$ (700 mg, 18.4 mmol) and then warmed to room temperature for 1 h. The reaction mixture was then concentrated under vacuum, and the resulting paste was dissolved in water (100 mL) and extracted with EtOAc (3 × 100 mL). The combined organics were washed with brine (50 mL), dried over MgSO$_4$, and concentrated and then flashed over silica gel (80% EtOAc:hexanes eluent, R_f = 0.15) to provide a white solid (557 mgs). The total material was redissolved in THF (10 mL) and added to a 0 °C solution of PPh$_3$ (1.23 g, 4.71 mmol), iodine (1.04 g, 4.08 mmol), and triethylamine (0.66 mL, 4.71 mmol). The reaction was maintained at room temperature overnight and then concentrated and purified by flash chromatography over silica gel (3−6% MeOH:DCM eluent) to provide a white solid which was dissolved in dioxane, treated with 1 N aq HCl, and heated to 50 °C for 2 h. The reaction was then concentrated and purified by reverse phase preparative HPLC to provide the isoxazoline **5** (224 mgs, 12% yield, 4 steps) as a white powder. ^{1}H NMR (400 MHz, 1.0 M DCl in D$_2$O) δ ppm 7.49 (s, 1 H), 5.17 (d, J = 2.3 Hz, 1 H), 4.61 (t, J = 1.0 Hz, 2 H), 3.67−3.82 (m, 3 H), 3.59−3.67 (m, 1 H), 3.46 (t, J = 1.0 Hz, 2 H). ^{13}C NMR (100 MHz, 1.0 M DCl in D$_2$O) δ ppm 146.88, 136.70, 135.53, 118.30, 73.09, 71.97, 71.02, 65.05, 63.21, 34.09. MS (EI) *m/z*: 258 [M + H]$^+$. HRMS calcd for C$_{10}$H$_{16}$N$_3$O$_5$ [M + H]$^+$ 258.1090, found 258.1073. HPLC (Sunfire C18 4.6 mm × 50 mm, 10 mM aq NH$_4$OAc, 8 min isocratic) t_R = 3.41 min, 100% integrated area.

(1R,2S,3R)-1-(2-(5-Ethoxyisoxazol-3-yl)-1H-imidazol-4-yl)-butane-1,2,3,4-tetraol (14). Prepared according to the general procedure A from 5-ethoxyisoxazole-3-carbonitrile (2.42 g, 17.52 mmol) and fructosamine−HOAc (4.19 g, 17.52 mmol) to provide **14** as the HCl salt (5.16 g, 88% yield). ^{1}H NMR (400 MHz, 1.0 M DCl in D$_2$O) δ ppm 7.44 (s, 1 H), 5.87 (s, 1 H), 5.11 (d, J = 1.3 Hz, 1 H), 4.27 (q, J = 7.1 Hz, 2 H), 3.49−3.78 (m, 4 H), 1.29 (t, J = 7.1 Hz, 3 H). ^{13}C NMR (101 MHz, 1.0 M DCl in D$_2$O) δ175.06, 150.95, 136.20, 134.30, 117.72, 77.07, 72.62,

70.51, 70.45, 64.51, 62.74, 13.48. MS (EI) *m/z*: 300 [M + H]$^+$. HRMS calcd for $C_{10}H_{13}N_3O_4S$ [M + H]$^+$ 300.1196, found 300.1185. HPLC (Luna Phenyl-hexyl 4.6 mm × 50 mm, 5% 10 mM aq NH$_4$OAc, 3 min isocratic) t_R = 2.49 min, 99% integrated area.

(1R,2S,3R)-1-(2-(5-Cyclopropylisoxazol-3-yl)-1H-imidazol-4-yl)butane-1,2,3,4-tetraol (10). Prepared according to the general procedure A from 5-cyclopropylisoxazole-3-carbonitrile (68 mg, 0.50 mmol) and fructosamine−HOAc (120 mg, 0.5 mmol) to provide **10** as the HCl salt (86 mg, 52% yield). ^{1}H NMR (400 MHz, 1.0 M DCl in D$_2$O) δ ppm 7.01 (s, 1 H), 6.03−6.07 (m, 1 H), 4.67 (s, 1 H), 3.17−3.30 (m, 3 H), 3.06−3.15 (m, 1 H), 1.56−1.66 (m, 1 H), 0.52−0.60 (m, 2 H), 0.42 (dd, *J* = 4.8, 2.5 Hz, 2 H). ^{13}C NMR (101 MHz, 1.0 M DCl in D$_2$O) δ ppm 179.11, 149.27, 135.85, 134.29, 117.77, 97.42, 72.59, 70.62, 64.50, 62.79, 8.70, 7.61. MS (EI) *m/z*: [MH]$^+$ 296 HRMS calcd for $C_{13}H_{18}N_3O_5$ [M + H]$^+$ 296.1246, found 296.1259. HPLC (Sunfire C18 4.6 mm × 50 mm, 5−90% [methanol/water/TFA (95/5/0.1)]:0.1% aq TFA, 2 min gradient) t_R = 0.59 min, 99% integrated area.

(1R,2S,3R)-1-(2-(5-Methyl-4-nitroisoxazol-3-yl)-1H-imidazol-4-yl)butane-1,2,3,4-tetraol (18). Prepared according to the general procedure A from 5-methyl-4-nitroisoxazole-3-carbonitrile (1.00 g, 6.54 mmol) and fructosamine−HOAc (1.55 g, 6.54 mmol) to provide **18** as the HCl salt (76 mg, 3% yield). ^{1}H NMR (400 MHz, 1.0 M DCl in D$_2$O) δ ppm 7.31 (s, 1 H), 4.93 (s, 1 H), 3.63−3.81 (m, 3 H), 3.49−3.57 (m, 1 H), 2.78 (s, 3 H). MS (EI) *m/z*: 315 [M + H]$^+$. HRMS calcd for $C_{11}H_{15}N_7O_7$ [M + H]$^+$ 315.0941, found 315.0952. HPLC (Sunfire C18 4.6 mm × 50 mm, 5−90% [methanol/water/TFA (95/5/0.1)]:0.1% aq TFA, 2 min gradient) t_R = 0.54 min, 98% integrated area.

(1R,2S,3R)-1-(2-(5-(Hydroxymethyl)isoxazol-3-yl)-1H-imidazol-4-yl)butane-1,2,3,4-tetraol (15). Prepared according to the general procedure A from 5-(hydroxymethyl)isoxazol-3-carbonitrile (244 mg, 1.17 mmol) and fructosamine−HOAc (279 g, 1.17 mmol) to provide **15** as the HCl salt (217 mg, 68% yield). ^{1}H NMR (400 MHz, 1.0 M DCl in D$_2$O) δ 7.23 (s, 1 H), 6.63 (s, 1 H), 4.88 (s, 1 H), 4.46 (s, 2 H), 3.36−3.53 (m, 3 H), 3.32 (s, 1 H). ^{13}C NMR (75 MHz, 1.0 M DCl in D$_2$O) δ ppm 174.40, 149.52, 136.17, 134.15, 117.93, 101.23, 72.66, 70.59, 64.55, 62.83, 54.83. MS (EI) *m/z*: [MH]$^+$ 286. HRMS calcd for $C_{11}H_{16}N_3O_6$ [M + H]$^+$ 286.1039, found 286.1056. HPLC (YMC-Pack ODS-A 4.6 mm × 50 mm, 10−95% [methanol/water/TFA (95/5/0.1)]:0.1% aq TFA, 4 min gradient) t_R = 0.44 min, 98% integrated area.

(1R,2S,3R)-1-(2-(5-((Dimethylamino)methyl)isoxazol-3-yl)-1H-imidazol-4-yl)butane-1,2,3,4-tetraol (16). Prepared according to the general procedure A from 5-((dimethylamino)methyl)-isoxazole-3-carbonitrile (215 mg, 1.42 mmol) and fructosamine−HOAc (339 mg, 1.42 mmol) to provide **16** as the HCl salt (126 mg, 25% yield). ^{1}H NMR (400 MHz, 1.0 M DCl in D$_2$O) δ 7.27 (s, 1 H), 7.05 (s, 1 H), 4.90 (s, 1 H), 4.38 (s, 2 H), 3.39−3.51 (m, 3 H), 3.27−3.35 (m, 1 H). ^{13}C NMR (75 MHz, 1.0 M DCl in D$_2$O) δ ppm 163.87, 150.26, 136.50, 133.35, 118.23, 107.31, 72.63, 70.57, 64.55, 62.81, 50.39, 43.05. MS (EI) *m/z*: 313 [M + H]$^+$. HRMS calcd for $C_{13}H_{21}N_4O_5$ [M + H]$^+$ 313.1512, found 313.1499. HPLC (YMC-Pack ODS-A 4.6 mm × 50 mm, 10−95% [methanol/water/TFA (95/5/0.1)]:0.1% aq TFA, 4 min gradient) t_R = 0.25 min, 100% integrated area.

(1R,2S,3R)-1-(2-(4-Ethylisoxazol-3-yl)-1H-imidazol-4-yl)-butane-1,2,3,4-tetraol (19). Prepared according to the general procedure A from 4-ethylisoxazole-3-carbonitrile (366 mg, 3.00 mmol) and fructosamine-HOAc (714 mg, 3.00 mmol) to provide **19** as the HCl salt (200 mg, 21% yield). ^{1}H NMR (400 MHz, 1.0 M DCl in D$_2$O) δ ppm 8.68 (s, 1 H), 7.58 (s, 1 H), 5.22 (d, *J* = 1.5 Hz, 1 H), 3.78 (s, 3 H), 3.58−3.67 (m, 1 H), 2.58 (q, *J* = 7.5 Hz, 2 H), 1.13 (t, *J* = 7.5 Hz, 3 H). MS (EI) *m/z*: 284 [M + H]$^+$. HRMS calcd for $C_{12}H_{18}N_3O_5$ [M + H]$^+$ 284.1246, found 284.1259. HPLC (Sunfire C18 4.6 mm × 50 mm, 10−90% MeCN:10 mM aq NH$_4$OAc, 2 min gradient) t_R = 0.77 min, 98% integrated area.

References

(1) (a) Vogel, P.; Donoviel, M. S.; Read, R.; Hansen, G. M.; Hazelwood, J.; Anderson, S. J.; Sun, W.; Swaffield, J.; Oravecz, T. Incomplete Inhibition of Sphingosine 1-Phosphate Lyase Modulates Immune System Function yet Prevents Early Lethality and Non-Lymphoid Lesions. *PloS ONE* **2009**, *4* (1), e4112. (b) Fyrst, H.; Saba, J. D. Sphingosine-1-phosphate lyase in development and disease: Sphingosine metabolism takes flight. *Biochim. Biophys. Acta* **2008**, *1781*, 448–458. (c) For a review, see: Kumar, A.; Saba, J. D. Lyase to live by: sphingosine phosphate lyase as a therapeutic target. *Expert Opin. Ther. Targets* **2009**, *13*, 1–13. (d) Weber, C.; Krueger, A.; Münk, A.; Bode, C.; Van Veldhoven, P. P.; Gräler, M. H. Discontinued postnatal thymocyte development in sphingosine 1-phosphate-lyase-deficient mice. *J. Immunol.* **2009**, *7*, 4292–4301. (e) Bektas, M.; Allende, M. L.; Lee, B. G.; Chen, W; Amar, M. J.; Remaley, A. T.; Saba, J. D.; Proia, R. L. Sphingosine 1-phosphate lyase deficiency disrupts lipid homeostatis in liver. *J. Biol. Chem.* **2010**, 10880–10889.

(2) (a) Reiss, U.; Oskouian, B.; Zhou, J.; Gupta, V.; Sooriyakumaran, P.; Kelly, S.; Wang, E.; Merrill, A. H.; Saba, J. D. Sphingosine-phosphate lyase enhances stress-induced ceramide generation and apoptosis. *J. Biol. Chem.* **2004**, *279*, 1281–1290. (b) Moore, A. N.; Kampfl, A. W.; Zhao, X.; Hayes, R. L.; Dash, P. K. Sphingosine 1-phosphate induces apoptosis of cultured hippocampal neurons that requires protein phosphatases and activator protein-1 complexes. *Neuroscience* **1999**, *94*, 405–415. (c) Maceyka, M. H.; Sankala, N. C.; Hait, H.; Le Stunff, H.; Liu, R.; Toman, C.; Collier, M.; Zhang, L. S.; Satin, A. H.; Merrill, S.; Milstien, S.; Spiegel, S. SphK1 and SphK2, sphingosine kinase isoenzymes with opposing functions in sphingolipid metabolism. *J. Biol. Chem.* **2005**, *280*, 37118–37129. (d) Pyne, S.; Pyne, N. J. Sphingosine 1-phosphate signalling in mammalian cells. *J. Biochem.* **2000**, *349*, 385–402. (e) McVerry, B.; Garcia, J. In vitro and in vivo modulation of vascular barrier integrity by sphingosine 1-phosphate: mechanistic insights. *Cell. Signalling* **2005**, 131–139. (f) Cyster, J. G. Chemokines, sphingosine-1-phosphate, and cell migration in secondary lymphoid organs. *Annu. Rev. Immunol.* **2005**, *23*, 127–159. (g) Hait, N. C.; Oskeritzian, C. A.; Paugh, S. W.; Milstien, S.; Spiegel, S. Sphingosine kinases, sphingosine 1-phosphate, apoptosis and diseases. *Biochim. Biophys. Acta* **2006**, *1758*, 2016–2026. (h) Rosen, H.; Goetzl, E. J. Sphingosine 1-phosphate and its receptors: an autocrine and paracrine network. *Nature Rev. Immunol.* **2005**, *5*, 560–570. (i) Saba, J. D.; Hla, T. Point−counterpoint of sphingosine 1-phosphate metabolism. *Circ. Res.* **2004**, *94*, 7240–7234.

(3) For a general review, see: (a) Marsolais, D.; Rosen, H. Chemical modulators of sphingosine-1-phosphate receptors as barrier oriented therapeutic molecules. *Nature Rev. Drug Discovery* **2009**, *8*, 297–307. (b) Goetzl, E. J.; Wang, W.; McGiffert, C.; Huang, M.-C.; Graeler, M. H. Sphingosine 1-phosphate and its G protein-coupled receptors constitute a multifunctional immunoregulatory system. *J. Cell. Biochem.* **2004**, *92*, 1104–1114. (c) Sanchez, T; Hla, T. Structural and functional characteristics of S1P receptors. *J. Cell. Biochem.* **2004**, *92*, 913–922. (d) Goetzl, E. J.; Liao, J.-J.; Huang, M.-C. Regulation of the roles of sphingosine 1-phosphate and its type 1 G protein-coupled receptor in T cell immunity and autoimmunity. *Biochem. Biophys Acta* **2008**, *1781*, 503–507. (e) Goetzl, E. J.; Rosen, H. Regulation of immunity by lysosphigolipids and their G protein-coupled receptors. *J. Clin. Invest.* **2004**, *114*, 1531–1537.

(4) (a) Cohen, J. A.; Barkhof, F.; Comi, G.; Hartung, H.-P.; Khatri, B. O.; Montalban, X.; Pelletier, J.; Capra, R.; Gallo, P.; Izquierdo, G.; Tiel-Wilck, K.; de Vera, A.; Jin, J.; Stites, T.; Wu, S.; Aradhye, S.; Kappos, L. Oral fingolimod or intramuscular interferon for relapsing multiple sclerosis. *N. Engl. J. Med.* **2010**, *362*, 402–415. (b) Adachi, K.; Kohara, T.; Nakao, N.; Masafumi, A.; Chiba, K.; Mishina, T.; Sasaki, S.; Fujita, T. Design, Synthesis, and Structure−Activity Relationships of 2-Substituted-2-Amino-1,3-Propanediols: Discovery of a Novel Immunosuppressant, FTY720. *Bioorg. Med. Chem. Lett.* **1995**, *5*, 853–856. (c) Chi, H.; Flavell, R. A. Cutting Edge: Regulation of T Cell Trafficking and Primary Immune Responses by Sphingosine 1-Phosphate Receptor 1. *J. Immunol.* **2005**, *174*, 2485–2488. (d) Wang, W.; Huang, M.-C.; Goetzl, E. J. Type 1 Sphingosine 1-Phosphate G

Protein-Coupled Receptor (S1P1) Mediation of Enhanced IL-4 Generation by CD4 T cells from S1P1 Transgenic Mice. *J. Immunol.* **2007**, *178*, 4885–4890.

(5) (a) For a comprehensive treatment, see: Brinkmann, V. Sphingosine 1-phosphate receptors in health and disease: mechanistic insights from gene deletion studies and reverse pharmacology. *Pharmacol. Ther.* **2007**, *115*, 84–105. (b) Maceyka, M.; Spiegel, S. Sphingosine-1-phosphate receptors. *Handb. Cell Signaling* **2004**, *2*, 247–251. (c) Oo, M. L.; Thangada, S.; Wu, M. T.; Liu, C. H.; Macdonald, T. L.; Lynch, K. R.; Lin, C. Y.; Hla, T. Immunosuppressive and anti-angiogenic sphingosine 1-phosphase receptor-1 agonists unduce ubiquitinylation and proteasomal degradation of the receptor. *J. Biol. Chem.* **2007**, *282*, 9082–9089. (d) Parrill, A. L.; Wang, D.; Bautista, D. L.; Van Brocklyn, J. R.; Lorincz, Z.; Fischer, D. J.; Baker, D. L.; Liliom, K.; Spiegel, S.; Tigyi, G. Identification of edg1 receptor residues that recognize sphingosine 1-phosphate. *J. Biol. Chem.* **2000**, *275*, 39379–39384. (e) LaMontagne, K.; Littlewood-Evans, A.; Schnell, C.; O'Reilly, T.; Wyder, L.; Sanchez, T.; Probst, B.; Butler, J.; Wood, A.; Liau, G.; Billy, E.; Theuer, A.; Hla, T.; Wood, J. Antagonism of sphingosine-1-phosphate receptors by FTY720 inhibits angiogenesis and tumor vascularization. *Cancer Res.* **2006**, *66*, 221–231. (f) Maceyka, M.; Milstein, S.; Spiegel, S. Sphingosine-1-phosphate: the Swiss army knife of sphingolipid signaling. *J. Lipid Res.* **2009**, S272–S276.

(6) Schwab, S. R.; Pereira, J. P.; Matloubian, M.; Xu, Y.; Huang, Y.; Cyster, J. G. Lymphocyte sequestration through S1P lyase inhibition and disruption of S1P gradients. *Science* **2005**, *309*, 1735–1739.

(7) (a) Bandhuvula, P.; Fyrst, H.; Saba, J. D. A rapid fluorescence assay for sphingosine-1-phosphate lyase enzyme activity. *J. Lipid Res.* **2007**, *48*, 2769–2778.

(8) Bagdanoff, J. T.; Donoviel, M. S.; Nouraldeen, A.; Tarver, J.; Fu, Q; Carlsen, M.; Jessop, T.; Zhang, H.; Hazelwood, H.; Nguyen, H.; Baugh, S. D. P.; Gardyan, M; Terranova, K. M.; Barbosa, J.; Yan, J.; Bednarz, M.; Layek, S.; Taylor, J.; Digeorge-Foushee, A. M.; Gopinathan, S.; Bruce, D.; Smith, T.; Moran, L.; O'Neill, E.; Kramer, J.; Lai, Z.; Kimball, S. D.; Liu, Q.; Sun, W.; Yu, S.; Swaffield, J.; Wilson, A.; Main, A.; Carson, K. G.; Oravecz, T.; Augeri, D. J. Inhibition of Sphingosine-1-Phosphate Lyase (S1PL) for the Treatment of Autoimmune Disorders. *J. Med. Chem.* **2009**, *52*, 3941–3953.

(9) (a) Hodge, J. E.; Rist, C. E. Amadori rearrangement under new conditions and its significance for nonenzymatic browning reactions. *J. Am. Chem. Soc.* **1953**, *75*, 316–322. (b) Hodge, J. E.; Fisher, B. E. In *Methods in Carbohydrate Chemistry*; Whistler, R. L., Wolfrom, M. L., Bemiller, J. N., Eds.; Academic Press: New York, 1963; Vol. II, pp 99−103.

(10) Buchi, G.; Halweg, K. M. A Convenient Synthesis of 2-Acetyl-4(5)-(1(R),2(S),3(R),4-tetrahydroxybutyl)-imidazole. *J. Org. Chem.* **1985**, *50*, 1134–1136.

(11) Conducting the reaction in methanol-d_4 reveals that deuterium is incorporated into the core imidazole ring. On the basis of this observation and in situ NMR experiments, a reasonable mechanism involves formation of the imidiate *B* from ethoxyacrylonitrile *A*. Subsequent condensation with fructosamine acetate **6** provides *C*, which equilibrates to deuterated intermediate *D* in the presence of excess methanol-d_4. Intramolecular cyclization to *E* preceeds aromatization and enol-ether hydrolysis to deuterated THI analogue d_1-**1**.

(12) Yu, X. Q.; Kramer, J.; Moran, L; O'Neill, E.; Nouraldeen, A.; Oravecz, T.; Wilson, A. Pharmacokinetic and Pharmacodynamic modeling of 2-acetyl-4(5)-tetrahydroxyimidazole-induced peripheral lymphocyte sequestration through increasing lymphoid sphingosine 1-phosphate. *Xenobiotica* **2010**, *40*, 350–356.

(13) Kondoh, M.; Yagi, K. Progress in absorption enhancers based on tight junction. *Expert Opin. Drug Delivery* **2007**, *4*, 275–286.

(14) (a) Van Veldhoven determined the catalytic turnover of S1PL in mammalian tissues and cultured cells to be between 20 and 100 pmol/min/mg protein. Internal unpublished results with full length protein including N-terminal membrane-binding region normally bound to endoplasmic reticulum supported these findings

and further internal study with a fluorogenic substrate, in addition to radioactively-labeled S-1-P, also supported slow catalytic turnover rates for S-1-P Lyase. For references, see: Van Veldhoven, P. P. Sphingosine-1-phosphate Lyase. *Methods Enzymol.* **1999**, *311*, 244–254. (b) Van Veldhoven, P. P.; Mannaerts, G. P. Sphingosine-Phosphate Lyase. *Adv. Lipid Res.* **1993**, *26*, 69–98. For fluorogenic substrate, see (c) Bedia, C.; Camacho, L.; Casas, J.; Abad, J. L.; Delgado, A.; Van Veldhoven, P. P.; Fabrias, G. Synthesis of a Fluorogenic Analogue of Sphingosine-1-Phosphate and Its Use to Determine Sphingosine-1-Phosphate Lyase Activity. *ChemBioChem* **2009**, *10*, 820–822.

(15) (a) Internal findings using FTY-720 as a positive control, unpublished results. (b) Phosphorylation of FTY720 is a facile process and synthetic agonist binds to S1PR on the cell surface of lymphocytes. For related published results, see: Foster, C. A.; Howard, L. M.; Schweitzer, A.; Persohn, E.; Hiestand, P. C.; Balatoni, B.; Reuschel, R.; Beerli, C.; Schwartz, M.; Billich, A. *J. Pharmacol. Exp. Ther.* **2007**, *323*, 469–476.

(16) (a) Queneau, P. The saga of aspirin: centuries-old ancestors of an old lady who doesn't deserve to die. *Therapie* **2001**, *56*, 723–726. (b) Miner, J.; Hoffhines, A. The discovery of aspirin's antithrombotic effects. *Texas Heart Inst. J.* **2007**, *34*, 179–186. (c) Mahdi, J. G.; Mahdi, A. J.; Madhi, A. J.; Bowen, I. D. The historical analysis of aspirin discovery, its relation to the willow tree and antiproliferative and anticancer potential. *Cell Proliferation* **2006**, *39*, 147–155.

(17) (a) Bentley, R. The development of penicillin: Genesis of a famous antibiotic. *Perspect. Biol. Med.* **2005**, *48*, 444–452. (b) Diggins, F. W. The true history of the discovery of penicillin, with refutation of the misinformation in the literature. *Br. J. Biomed. Sci.* **1999**, *56*, 83–93.

(18) For a general review, see: Masataka, Y. Iodine and Living Body. *Kagaku Keizai* **2008**, *55*, 75–80.

(19) (a) Fujita, T.; Yoneta, M.; Hirose, R.; Sasaki, S.; Inoue, K.; Kiuchi, M; Hirase, S.; Adachi, K.; Arita, M.; Chiba, K. Simple compounds, 2-alkyl-2-amino-1,3-propanediols have potent immunosuppressive activity. *Bioorg. Med. Chem. Lett.* **1995**, *5*, 847–852. (b) Adachi, K.; Kohara, T.; Nakao, N.; Masafumi, A.; Chiba, K.; Mishina, T.; Sasaki, S.; Fujita, T. Design, Synthesis, and Structure−Activity Relationships of 2-Substituted-2-Amino-1,3-Propanediols: Discovery of a Novel Immunosuppressant, FTY720. *Bioorg. Med. Chem. Lett.* **1995**, *5*, 853–856. (c) Kiuchi, M.; Adachi, K.; Kohara, T.; Teshima, K.; Masubuchi, Y.; Mishina, T.; Fujita, T. Synthesis and biological evaluation of 2,2-disubstituted 2-aminoethanols: analogues of FTY720. *Bioorg. Med. Chem. Lett.* **1998**, *8*, 101–106.

(20) (a) Bagli, J. F.; Kluepfel, D. Elucidation of Structure and Stereochemistry of Myriocin. A Novel Antifungal Antibiotic. *J. Org. Chem.* **1973**, *38*, 1253–1260. (b) Bagli, J. F.; Kluepfel, D.; St.-Jacques, M. Edlucidation of Structure and Stereochemistry of Myriocin. A Novel Antifungal Antibiotic. *J. Org. Chem.* **1973**, *38*, 1253–1260.

(21) (a) Miyake, Y.; Kozutsumi, Y.; Nakamura, S.; Fujita, T.; Kawasaki, T. Serine palmitoyltransferase is the primary target of a sphingosine-like immunosuppressant, ISP-1/ myriocin. *Biochem. Biophys. Res. Commun.* **1995**, *211*, 396–403. (b) Chen, J. K.; Lane, W. S.; Schreiber, S. L. The identification of myriocin-binding proteins. *Chem. Biol.* **1999**, *6*, 221–235.

(22) Brinkmann, V.; Davis, M. D.; Heise, C. E.; Albert, R.; Cottens, S.; Hof, R.; Bruns, C.; Prieschl, E.; Baumruker, T.; Hiestand, P.; Foster, C. A.; Zollinger, M.; Lynch, K. R. The immune modulator FTY720 targets sphingosine 1-phosphate receptors. *J. Biol. Chem.* **2002**, *277*, 21453–21457.

(23) (a) Rivera, J.; Proia, R. L.; Olivera, A. The alliance of sphingosine-1-phosphate and its receptors in immunity. *Nature Rev. Immunol.* **2008**, *8*, 753–763. (b) Billich, A.; Baumruker, T.; Sphingolipid Metabolizing Enzymes as Novel Theraputic Targets. In *Lipids in Health and Disease*; Quinn, P. J., Wang, X., Eds.; Springer Science Business Media BV: New York, 2008; pp487−522.

(24) (a) Peng, X.; Hassoun, P. M.; Sammani, S.; McVerry, B. J.; Burne, M. J.; Rabb, H.; Pearse, D.; Tuder, R. M.; Garcia, J. G. N. Protective effects of sphingosine 1-phosphate in murine endotoxin-induced inflammatory lung injury. *Am. J. Respir. Crit. Care Med.* **2004**, *169*, 1245–1251. (b) Nofer, J. R.; van der Giet, M.; Tolle, M.; Wolinska, I.; von Wnuck Lipinski, K.; Baba, H. A.; Tietge, U. J.; Godecke, A.; Ishii, I.; Kleuser, B.; Schafers, F.; Fobker, M; Zidek, W.; Assmann, G.; Chun, J.; Levkau, B. HDL induces NO-dependent vasorelaxation via the lysophospholipid receptor S1P3. *J. Clin. Invest.* **2004**, *113*, 569–581. (c) Van der Giet, M.; Tolle, M.; Kleuser, B. Relevance and potential of sphingosine-1-phosphate in vascular inflammatory disease. *Biol. Chem.* **2008**, *389*, 1381–1390.

(25) Hughes, J. E.; Srinivasan, S.; Lynch, K. R.; Proia, R. L.; Ferdek, P.; Hedrick, C. C. Sphingosine-1-phosphate induces an antiinflammatory phenotype in macrophages. *Circ. Res.* **2008**, *102*, 950–958.

(26) Rolin, J.; Sand, K. L.; Knudsen, E.; Maghazachi, A. A. FTY720 and SEW2871 reverse the inhibitory effect of S1P on natural killer

cell mediated lysis of K562 tumor cells and dendritic cells but not on cytokine release. *Cancer Immunol. Immunother.* **2010**, *59*, 575–586.

(27) (a) Augeri, D. J. Inhibition of Sphingosine-1-Phosphate Lyase for the Treatment of Autoimmune Disorders. First Disclosure of LX2931/LX2932. 239th ACS National Meeting, San Francisco, CA, March 21−25, 2010, MEDI-36. (b) Fleischmann, R.; Frazier, K.; Freiman, J.; Brooks, B.; Donoviel, M.; Oravecz, T.; Augeri, D.; Heydorn, W.; Kelly, M.; Brown, P. Co-Administration of the Oral S1P-Lyase Inhibitor LX2931 with Methotrexate was Well Tolerated Over 14 Days in Patients with Stable Rheumatoid Arthritis. Meeting of the American College of Rheumatology, Philadelphia, PA, October 18, 2009, abstract 426.

(28) See experimental section of: Salojin, K.; Owusu, R. B.; Millerchip, K. A.; Potter, M.; Platt, K. A.; Oravecz, T. Essential Role of MAPK Phosphatase-1 in the Negative Control of Innate Immune Responses. *J. Immunol.* **2006**, *176*, 1899–1907.

(29) Isoxazole-3-carbonitrile synthesized by following procedure: Ethyl vinyl ether (75 mL, 1.35 mol) was added dropwise over 30 min to neat ethyl cholorooxoacetate cooled to 0 °C. The cooling bath was left in place, and the reaction was allowed to gradually warm to room temperature overnight. The excess ethyl vinyl ether was removed by rotovap, and then crude reaction was distilled rapidly (bp 102−104 °C, 9 Torr) to provide the vinylogous ester (68.8 g, 59% yield) as a clear liquid. Note: failure to initiate distillation within a few minutes of heating will result in polymerization of crude material. Therefore, it is recommended that the heating bath is ramped quickly above ∼150 °C while externally heating a well-insulated distillation head with a heat gun. To a room temperature solution of the resulting vinylogous eneone (260.0 g, 1.51 mol) in MeOH (1.5 L) was added hydroxylamine hydrochloride (110.0 g, 1.59 mol) in one portion. After 2 h, ^{1}H NMR of an aliquot of the reaction mixture indicated complete consumption of the starting material. The reaction was concentrated, and then the resulting oil was redissolved in chloroform (1 L). The solids were filtered off, and the liquor was concentrated. The resulting oil was azeotroped with methanol (2 × 1 L) to chase off trace chloroform. The crude material was used immediately in the next transformation. The oil was redissolved in methanol (1.5 L) and then treated with 25% w/w NaOMe (33.0 mL, 0.15 mol). After 1 h, ^{1}H NMR of an aliquot of the reaction mixture indicated complete conversion. The reaction mixture was then treated with a 7N solution of ammonia in MeOH. After 1 h, the reaction was concentrated to dryness. The resulting dark solid mass was pulverized with a mortar and pestle and then slurried in water (500 mL) and filtered to remove to provide, after rigorous drying, an orange solid which was used directly in the next reaction. The dried solid was slurried in DCM (1.5 L) and cooled to 0 °C and treated with pyridine (303.0 mL, 3.75 mol) while maintaining the internal temperature of the reaction below 10 °C. To the cooled solution, trifluoroacetic acid anhydride was added slowly through an addition funnel, again while carefully monitoring the internal temperature of the reaction. Once the addition was complete, the reaction was allowed to warm to room temperature for an hour before quenching with water (1 L). The aqueous layer was adjusted to pH = 2, and then the biphasic mixture was agitated. The aqueous layer was readjusted to pH = 2. The layers were separated, and the organics were washed with water (2 × 500 mL) and brine (500 mL) and then dried over MgSO$_4$. The resulting crude liquid was distilled (bp 81−83 °C, 31 tor) to provide the nitrile (82.0 g, 58% yield, 4 steps) as a colorless liquid. ^{1}H NMR (300 MHz, CDCl$_3$) δ ppm 8.70 (d, *J* = 1.5 Hz, 1 H), 6.77 (d, *J* = 1.2 Hz, 1 H). ^{13}C NMR (101 MHz, CDCl$_3$) δ ppm 160.92, 138.92, 109.81, 107.24.